

ON THE DISTRIBUTION OF PITCH ANGLES IN EXTERNAL GALACTIC SPIRALS NGC 1232 AND NGC 5457

WILLIAM S. RUSSELL¹ AND WILLIAM W. ROBERTS, JR.

Department of Applied Mathematics, Thornton Hall, University of Virginia, Charlottesville, VA 22903-2442

Received 1992 February 19; accepted 1992 April 14

ABSTRACT

A numerical method, originally developed to analyze the morphology of global and local structure in prototype galaxies, is modified for analyzing observed disk-shaped galaxies. Two digitized spiral galaxies NGC 1232 and NGC 5457 with varying degrees of contrast between arm and interarm regions are analyzed. A synergism of partitioning methods and a geometric mean least-squares regression algorithm serves to isolate local arm segments, spurs, feathers, and secondary features and to measure their pitch angles and lengths. The global arms are actually highly disjointed, with arm segments frequently revealing pitch angles between 30° and 50°, certainly greater than those of the parent arms. Prominent spurs tend to exhibit a much greater pitch angle. The automated mathematical algorithm is shown to have negligible numerical biasing and could be applied to any number of spiral galaxies manifesting flocculent structure, either prototype or observed, and could possibly be used as a tool for classification of multiple-armed-type galaxies.

Subject headings: galaxies: individual (NGC 1232, NGC 5457) — galaxies: spiral

1. INTRODUCTION

Multiple-armed external spiral galaxies exhibit flocculent structure. The spiral inhomogeneities can be classified as arm segments, spurs, feathers, bridges, or other general secondary features. It has been observed that global spiral arms are actually composed of a sequence of secondary type features, but a quantitative analysis of these isolated independent segments has never been undertaken for observed galaxies through numerical modeling techniques. This paper introduces an automated mathematical method to investigate morphological characteristics of the spiral structure on local and intermediate scales in multiple-armed galaxies NGC 1232 and NGC 5457. The emphasis, however, is to demonstrate the versatility of this mathematical method as a tool to analyze any number of external spiral galaxies of this type.

Lynds (1970) made studies of the dust lane widths and dark feathers that occurred in Sc-type galaxies. More recently Elmegreen (1979, 1980) made approximate measurements of length, width, and pitch angle of primary spurs appearing in a variety of spiral galaxies. The estimated error was $\pm 5^\circ$ since uncertainties arose in precisely defining the edges of features and also led to errors of the order 0.1 kpc in length and width approximations. In an attempt to address obvious questions such as “what constitutes a feature; how are edges of features defined; how can the pitch angle and length be measured accurately?” an automated mathematical method is formulated herein.

In mathematical-computational simulations carried out by Roberts et al. (1992; see also Roberts, Lowe, & Adler 1990; Adler & Roberts 1992) which follow the dynamics of 10,000–50,000 gas clouds, it was discovered that the gaseous self-gravity was instrumental in creating strong density inhomogeneities along spiral arms and in forming various types of interesting secondary spiral features (Roberts & Adler 1989). The morphological characteristics of this flocculent

structure are of great interest. Each gas cloud in their computer simulations represented a giant molecular cloud (of 10^6 – 10^7 solar masses or so). Hence, our automated mathematical method was first developed for analyses on distributions of N such clouds (Russell & Roberts 1992).

The N -body distribution is first partitioned into distinct features, and the lengths and pitch angles of these various features are then measured. To isolate the prominent features, methods are employed which are based on the premise that regions of high luminosity (equivalently, high star/cloud concentration) constitute features. Hence, if clouds contributing to a dense region can be ascertained, the associated feature can be effectively modeled. A geometric mean regression least-squares analysis (minimization of perpendicular distances, not vertical deviations) is then employed in a $(\ln r, \theta)$ coordinate system to approximate the pitch-angle value and length of each feature. The logarithmic spiral (log-spiral) $r = r_0 e^{\theta/p}$ has the attractive property of constant pitch angle. The synergism of the partitioning algorithms and the least-squares procedure has already been examined on a prototype galaxy taken from the multiparameter space, theoretical-computational studies of Roberts et al. (1992) where spiral properties were fairly easy to compute (Russell 1991; Russell & Roberts 1992).

An obvious question arises as to whether this automated method can be applied successfully to real external galaxies. Elmegreen, Elmegreen, & Seiden (1990) made studies of NGC 1232 and NGC 5457 and were kind enough to make available digitized data samples of the galaxies. Figures 1a and 1b show two images of NGC 1232 (produced by multiplying by two different accentuating factors) after a deprojection which renders the galactic image perpendicular to our line of sight. Each image reveals the abundance of spurs, bridges, arm segments and other prominent secondary features evident in photographs of this multiple-armed-type galaxy. Originally our automated method was not designed to be applied to an array of luminosities. However, by numerically transforming these luminosity arrays into distributions of N stellar associations, the original method can be applied directly (N represents the

¹ Postal address: NASA Goddard, Institute for Space Studies, 2880 Broadway, New York, NY 10025-7819.

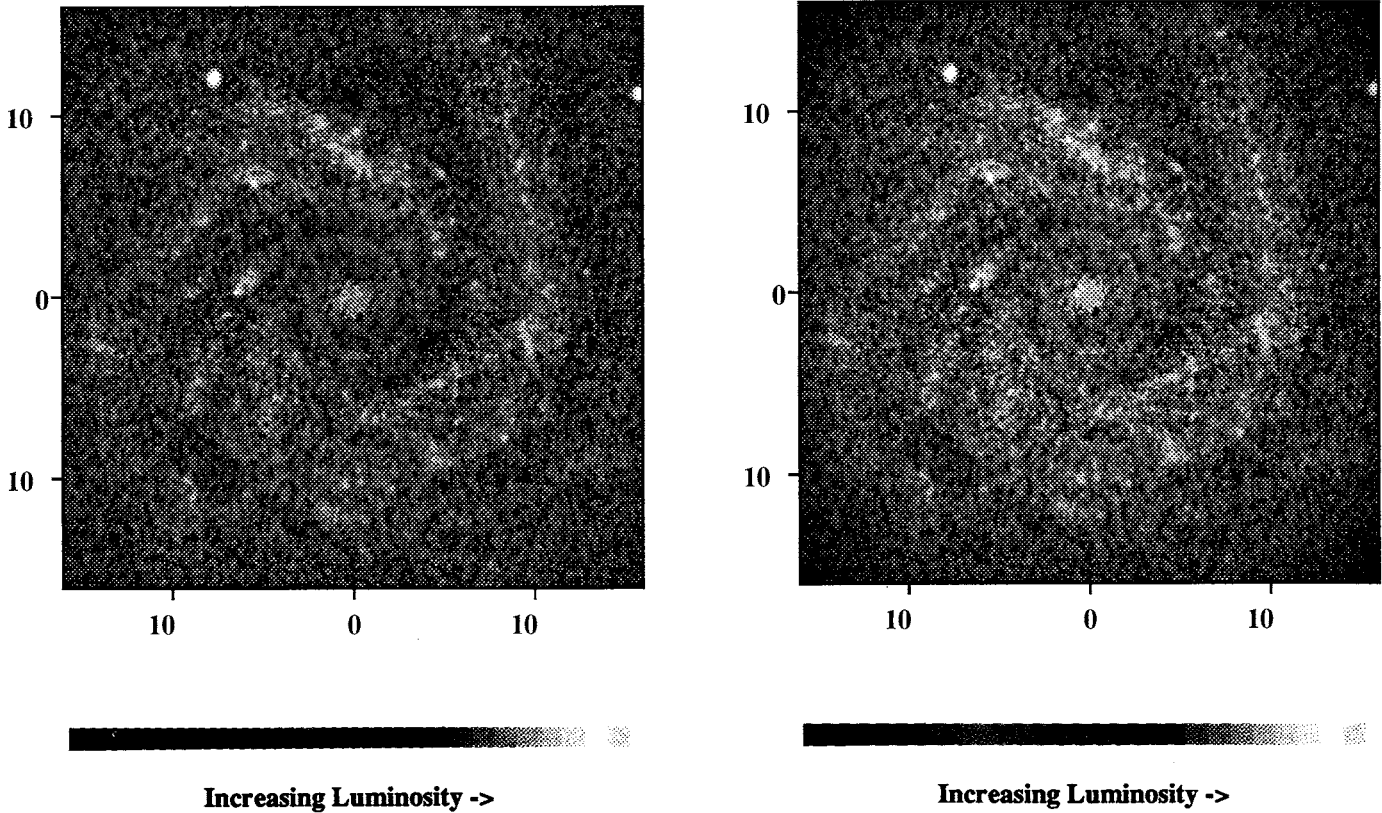


FIG. 1.—Photographic intensity maps of external spiral NGC 1232. The luminosity array (supplied by Elmegreen et al. 1990, and now published in the recent work of Elmegreen et al. 1992) is multiplied by radial factors (a) $[35-r]$, and (b) $[25-r]$ in order to accentuate the nonaxisymmetric part (i.e., secondary features) of the spiral galaxy.

number of stellar associations in the overall N -body calculation).

The complete numerical method developed by Russell (1991) is described briefly in § 2. In § 3 spiral loci of secondary features are presented along with the distributions of pitch angle weighted by feature lengths and masses. Comparisons are made between the distributions resulting from the various transformation algorithms (i.e., algorithms transforming original luminosity arrays to distributions of N stellar associations). Section 4 draws conclusions on the secondary structure for two real spiral galactic systems: NGC 1232 and NGC 5457.

2. MATHEMATICAL METHOD

Two automated partitioning algorithms are formulated so that any spiral galactic disk, either real or simulated in the form of an N -body distribution, can be separated into features, spurs, bridges, and other secondary features to allow computation of properties such as length, width, and pitch angle. These partitioning methods yield features in the form of sets of \mathcal{N} stellar association or cloud positions. (\mathcal{N} represents the number of stellar associations in any given feature.) A least-squares algorithm (based on the geometric mean regression analysis) is employed in a $(\ln r, \theta)$ coordinate system to capture the natural spiral shape of each feature. Finally, real digitized galaxy data in the form of luminosity arrays are transformed into an N -body distribution similar to those produced by Roberts et al. (1992).

2.1. The Partitioning Algorithms

To isolate the distinct features in the spiral galactic disk, a mathematical modeling technique, referred to here as *partitioning*, is employed to separate the stellar distribution (similarly gas cloud distribution for prototype galaxies) into areas of high density which constitute secondary features. Two algorithms for generating these features are compared.

Clouds in regions of high density necessarily have closer neighboring clouds than those in sparse regions. This provides the foundation of the first method; the distance tolerance (d_{tol}) algorithm. Clouds are assumed to contribute to features if and only if they have a sufficient number of neighboring clouds within a given distance tolerance. These clouds are then assigned to a distinct dense region of the galaxy. The resulting dense regions are treated as individual features. However, comparing distances between clouds is intuitively an $O(N^2)$ algorithm. For $N = 10,000$ this is computationally unacceptable. The d_{tol} algorithm can be successfully implemented by making use of a “small cell/big cell” technique substantially reducing the number of operations (details can be found in Russell 1991 and Russell & Roberts 1992).

The problem of choosing an appropriate value of d_{tol} is overcome by noting that wavelength of the global spiral arms varies approximately linearly as a function of galactic radius suggesting the use of a monotonically increasing function of radius, that is,

$$d_{\text{tol}} = \zeta r, \quad (1)$$

where ζ is a constant. Since it is difficult to distinguish which clouds truly contribute to a given feature, a sequence of tolerance values (ζ -values) is used to capture the complete spectrum of feature densities.

A second clumping algorithm, the a_{tol} algorithm, is based on Voronoi's theory (Voronoi 1908; see also Dirichlet 1850) that every cloud owns a certain portion of space in the shape of a polyhedron. These polyhedra are intersections of half-spaces and are always convex. Further, they partition in a unique way with the resulting diagram formally called the Voronoi diagram. Once the Voronoi diagram is constructed using a method developed by Brostow, Dussault, & Fox (1978; see also Russell 1991), it becomes apparent that small-area polyhedra are associated with clouds in dense regions and large-area polyhedra with clouds in sparse regions. By eliminating all clouds with associated area greater than some tolerance a_{tol} , only clouds lying in dense regions are retained. Each cloud is then assigned to a unique dense region interpreted as a feature.

In the same manner that a value or expression for d_{tol} was chosen, an expression for a_{tol} (the tolerance level at which areas of the Voronoi polyhedra are thrown away) must also be chosen. Since the wavelength increases linearly with r , and d_{tol} was chosen as a linear function of r , we conclude that the natural extension for a_{tol} is a function of r^2 : in particular

$$a_{\text{tol}} = \pi \left(\frac{\zeta r}{2} \right)^2 \quad (2)$$

with the same sequence of ζ -values.

2.2. The Least-Squares Algorithms

The pitch angle must somehow be approximated, given a distribution of \mathcal{N} cloud positions (x_i, y_i) contributing to each feature. Standard least squares searches for a fit of the form

$$\hat{y} = \hat{\alpha} + \hat{\beta}x. \quad (3)$$

The interest is in the orientation of the cloud set, that is, the value of $\hat{\beta}$. It quickly became apparent that using linear least squares did an inadequate job of approximating the pitch angle of the longer features. Hence a more accurate least-squares approach was developed which could cope with the curvature of the longer spurs and spiral arms, as well as the shorter secondary features.

Least-squares estimates are developed which fit log-spirals through the features. A best-fit curve of the form

$$r = r_0 \exp \left(\frac{\theta}{p} \right) \quad (4)$$

is required, where p is the pitch-angle parameter for the feature being analyzed in the least-squares calculation and θ increases with r along a spiral arm. Equivalently,

$$\theta = \hat{\alpha} + \hat{\beta} \ln r, \quad (5)$$

where $\hat{\alpha} = -p \ln r_0$ and $\hat{\beta} = p$.

There is clearly one distinct best-fit curve which minimizes the various least-squares error functions; the geometric mean. Hence we minimize the perpendicular error in $(\ln r, \theta)$ space

$$Q_1^s = \sum_{i=1}^{\mathcal{N}} (e_{\perp})_i^2 = \sum_{i=1}^{\mathcal{N}} \frac{[\theta_i - (\hat{\alpha} + \hat{\beta} \ln r_i)]^2}{1 + \hat{\beta}^2}. \quad (6)$$

Differentiating partially with respect to $\hat{\alpha}$ and $\hat{\beta}$ and equating to zero yields

$$\hat{\beta}^2 - 2T\hat{\beta} - 1 = 0, \quad (7)$$

where

$$T = \frac{1}{2} \left[\frac{\mathcal{N} \sum_{i=1}^{\mathcal{N}} \ln r_i^2 - (\sum_{i=1}^{\mathcal{N}} \ln r_i)^2}{\sum_{i=1}^{\mathcal{N}} \ln r_i \sum_{i=1}^{\mathcal{N}} \theta_i + (\sum_{i=1}^{\mathcal{N}} \theta_i)^2} \right]. \quad (8)$$

The solutions to equation (7) are

$$\hat{\beta} = T \pm (T^2 + 1)^{1/2}. \quad (9)$$

Note that the regression coefficient in equation (5) becomes

$$\hat{\alpha} = -\hat{\beta} \frac{1}{\mathcal{N}} \sum_{i=1}^{\mathcal{N}} \ln r_i + \frac{1}{\mathcal{N}} \sum_{i=1}^{\mathcal{N}} \theta_i. \quad (10)$$

It follows that the pitch angle $i_0 = \tan^{-1}(1/\hat{\beta})$.

Given θ_1 and θ_2 (the extreme axial points of the feature) the length can be expressed as

$$s = K \left[\exp \left(\frac{\theta_2}{\hat{\beta}} \right) - \exp \left(\frac{\theta_1}{\hat{\beta}} \right) \right], \quad (11)$$

where $K = (\hat{\beta}^2 + 1)^{1/2} \exp[-\hat{\alpha}/\hat{\beta}]$ and $\hat{\beta}$ nonzero.

An inaccurate least-squares estimate will strongly affect the final pitch-angle distribution; these inaccuracies must be detected and eliminated from any further analysis. The Kolmogorov-Smirnov test provides a formal procedure for checking whether results from least-squares analyses do in fact agree with underlying probabilistic model assumptions for the original data. The K-S test examines whether indeed the distributions of errors are normally distributed with mean zero.

The K-S test is performed in both $(\ln r, \theta)$ space and (x, y) space. The errors are given, respectively, as

$$E_i^s = \frac{\theta_i - (\hat{\alpha} + \hat{\beta} \ln r_i)}{(1 + \hat{\beta}^2)^{1/2}}, \quad E_i^c = \frac{d_r d_\theta}{(d_r^2 + d_\theta^2)^{1/2}}, \quad (12)$$

where

$$\begin{aligned} d_r &= r_i - \exp[(\theta_i - \hat{\alpha})/\hat{\beta}], \\ d_\theta &= r_i |\theta_i - (\hat{\alpha} + \hat{\beta} \ln r_i)|. \end{aligned} \quad (13)$$

If, for both of the distributions of errors, the modified form of the K-S statistic is greater than the 0.01 tolerance level, the least-squares estimate of the pitch angle is eliminated.

2.3. Transformation of Digitized Data

The NGC 1232 and NGC 5457 data samples (Elmegreen et al. 1990) were made available in the form of 512×512 arrays where each array entry represents the luminosity of a small square of the galaxy photographs. Since the analyses so far have been applied to distributions of N gas clouds, it would seem appropriate to perform the analysis of both NGC 1232 and NGC 5457 on a distribution of N stellar associations, rather than a distribution of 512×512 intensity values. Although in the future it would be desirable, when analyzing real galaxies, to formulate an algorithm that could scan a matrix of intensities, then locate and analyze various properties of distinct secondary features, it is more straightforward here to transform the luminosity values into a distribution of N stellar associations and proceed with that analysis developed originally for prototype galaxies.

The original NGC 1232 data sample had the axisymmetric portion of the galaxy removed. This was achieved by averaging the luminosities in successive annuli of the galactic domain and subtracting out the mean, leaving the nonaxisymmetric part of the galaxy, serving to accentuate the global spiral arms, spurs,

feathers, and other secondary features. Within each annulus, the nonaxisymmetric component became more prominent. However, comparing the resulting luminosity values from one annulus to the next is incorrect since their associated mean values are independent.

Hence, the logical method for transforming the luminosity array into a distribution of stellar associations, that is, sorting the luminosity values into descending order and skimming off the greatest N values (in which the $[m, n]$ coordinates associated with the greatest N luminosity values would be assumed to represent the positions of stellar associations) is highly unsatisfactory.

An obvious alternative choice of transformation is to calculate the mean μ and variance σ^2 of the luminosities for successive annuli and distribute more stellar associations at values of higher luminosity. At greater galactic radii, rather too many stellar associations are distributed. As a result, an application of the Voronoi partitioning (a_{vol}) algorithm produces features modeled at greater r than are really seen. Furthermore, due to the sparseness of stellar associations toward the center of NGC 1232, no features are modeled here. A more accurate transformation procedure had to be formulated.

It is evident that the spiral structure toward the center of NGC 1232 had been lost. By multiplying the luminosities by a factor $[\alpha - r]$ where r is the galactic radius (in kpc) of the luminosity location, luminosities close to the center could be accentuated and those with $r > \alpha$ eliminated. Calculating the mean μ and standard deviation σ of these altered luminosity values allows the distribution of stellar associations to depend directly on the value of the luminosity above the mean. More simply, if $l_{m,n} \in (\mu + (J + 1)\sigma, \mu + (J + 2)\sigma)$, then J stellar associations are distributed randomly around coordinate (m, n) .

Various values of α were tested and after some review, values of $\alpha = 35$ and 25 were chosen. As expected, the $\alpha = 25$ (henceforth $[25-r]$) case accentuates the central portion of the

galaxy rather more than the $\alpha = 35$ (or $[35-r]$) case. The mathematical computational models are now applied to the distributions of stellar associations representing NGC 1232 and NGC 5457, and pitch-angle distributions compared.

3. RESULTS

Multiple-armed spiral galaxies NGC 1232 and NGC 5457 in the form of digitized data supplied by Elmegreen et al. (1990) are analyzed for pitch-angle spectra. Both spiral galaxies exhibit flocculent structure, but after inspection of photographic intensity maps of the original luminosity arrays it is evident that the contrast between ridges and valleys for NGC 5457 is much stronger. To aid accentuation of the nonlinear component, the data samples are modified by multiplying by factors $[35-r]$ and $[25-r]$; both partitioning algorithms are employed on the resulting stellar distributions. Hence, for each galaxy four procedures are investigated for modeling secondary features. The interest is in determining whether the method described in Russell & Roberts (1992) can successfully predict the pitch-angle distribution for spiral features in observed galaxies; whether confidence can be put in the results, that is, can speculation be dispelled as to whether primary characteristics borne out of resulting pitch-angle distributions are numerically dependent; and to investigate the differences in the characteristics of the pitch angle distributions for fuzzy versus well-delineated spiral structure in external spirals.

The $[35-r]$ transformed version of NGC 1232 is shown in Figure 1a. The associated N -body distribution consists of almost 10,000 stellar associations, approximately one-quarter of which are shown in Figure 2a. For simple comparison, the equivalent $[25-r]$ intensity map and N -body distribution are given in Figures 1b and 2b, respectively. For the $[35-r]$ case the a_{vol} partitioning algorithm is first employed to isolate each of the prominent features. For each distinct feature the pitch angle, length, and mass are calculated. Figure 3a identifies the least-squares spiral loci of the more prominent features. The

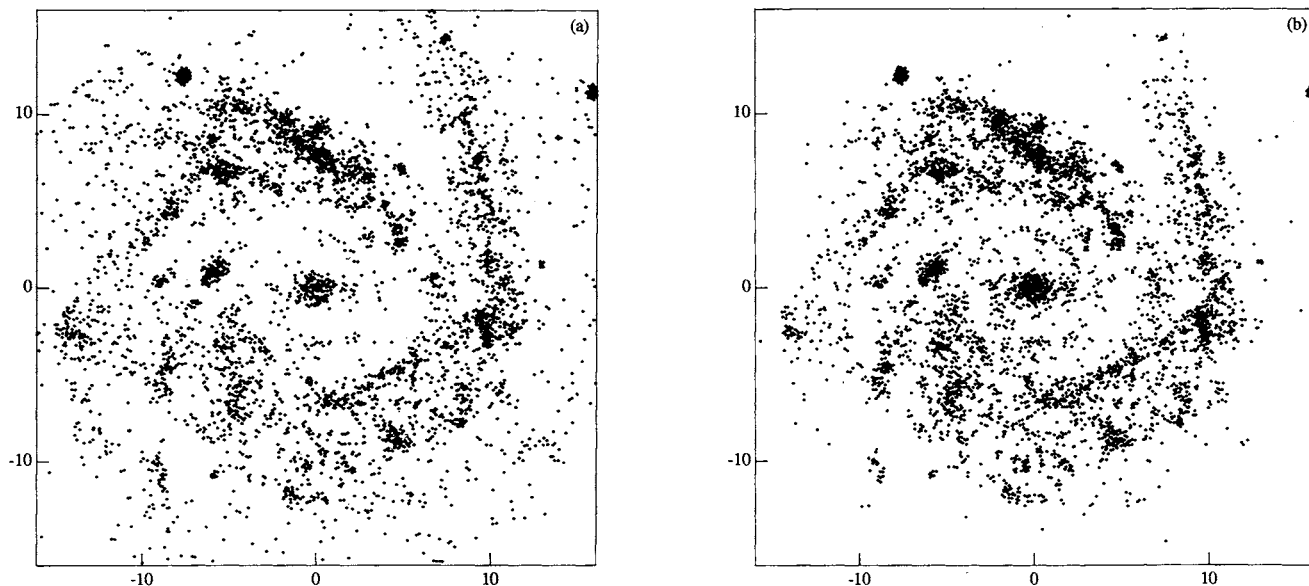


FIG. 2.— N -body distributions representing NGC 1232 transformed from the photographic intensity maps shown in Fig. 1 (a) after multiplication by the $[35-r]$ factor, and (b) after multiplication by the $[25-r]$ factor. The $[35-r]$ case tends to enhance features lying further from the galactic center, whereas the $[25-r]$ case includes more toward the center. Only one-quarter of the approximate by 10,000 star locations used in our analyses are plotted here.

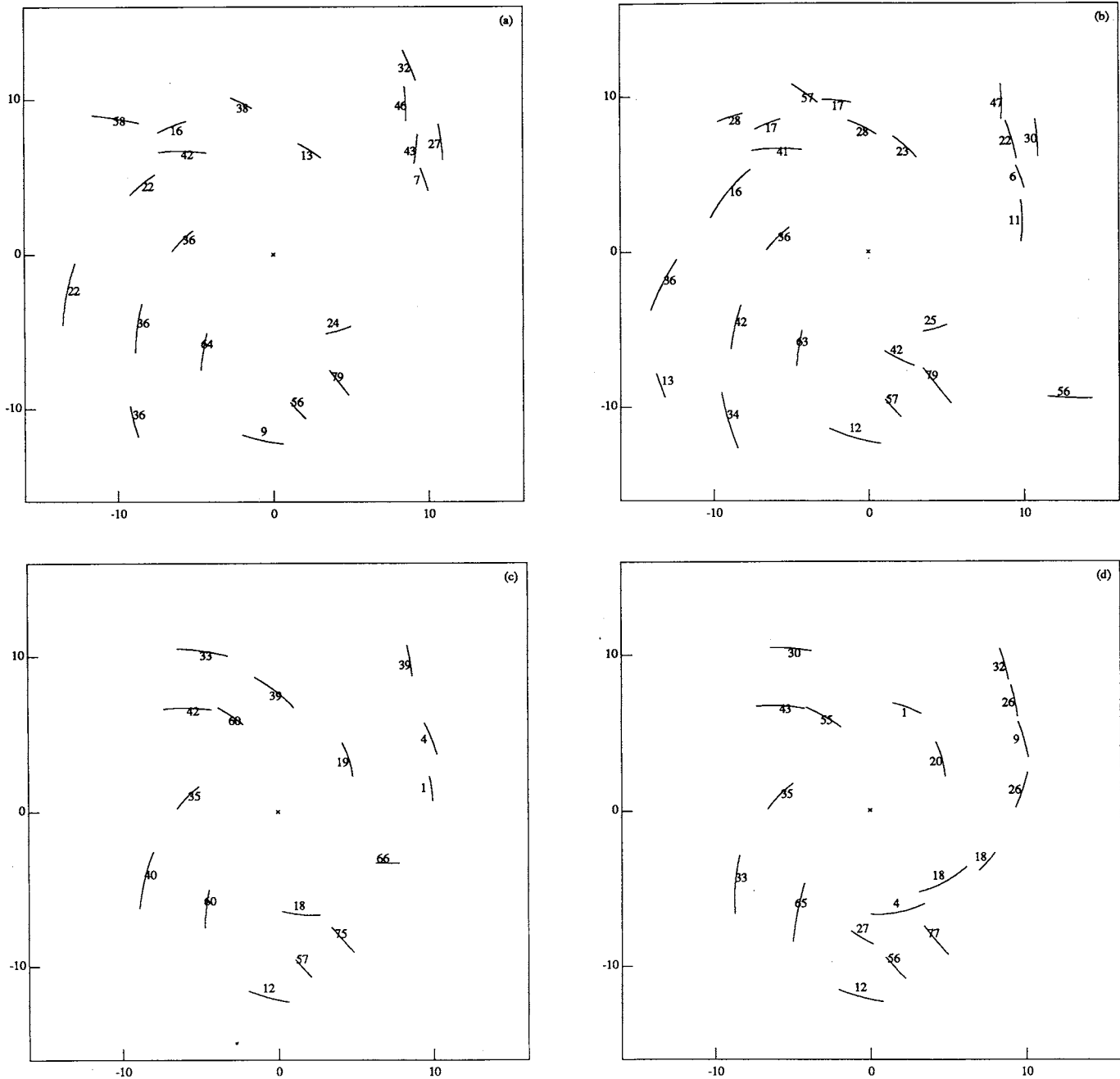


FIG. 3.—Prominent spiral loci (i.e., at least 1.5 kpc long) for NGC 1232. The a_{l01} partitioning algorithm is applied to the N -body distribution associated with [35- r] case (a), and the loci represent the least-squares geometric mean regression fits. The numbers represent pitch-angle values to the nearest degree. Spiral loci for the [35- r] case after employment of the d_{l01} algorithm are shown in graph (b). (c) and (d) Spiral loci for the [25- r] case after employing the a_{l01} and d_{l01} algorithms, respectively.

arms branch continuously, but the primary arm segments have been accurately modeled.

The distribution of pitch angles is determined by taking each integer value of i_0 , and summing the number of stellar associations contributing to features with pitch angles between $i_0 \pm 2.5$ over all values of ζ . Also, weighting by the number of stellar associations in, or equivalently the mass of, each feature results in dense features becoming more significant. This binning and averaging approach, although effectively smoothing the pitch-angle distribution, seems more appropriate since

the pitch-angle values computed are not exact, but merely good approximations. In the pitch-angle distributions in, for example, Figure 4a, the top curve is the overall distribution; the middle curve considers only those features of length greater than 1 kpc, and the lower curve those greater than 1.5 kpc. Hence the lower curve in Figure 4a supplies the most useful information concerning long, dense, and consequently most prominent features. Two primary peaks near 35° and 45° , a secondary peak near 80° , and less prominent peaks near 22° and 64° appear. The lower curve indicates that many of the

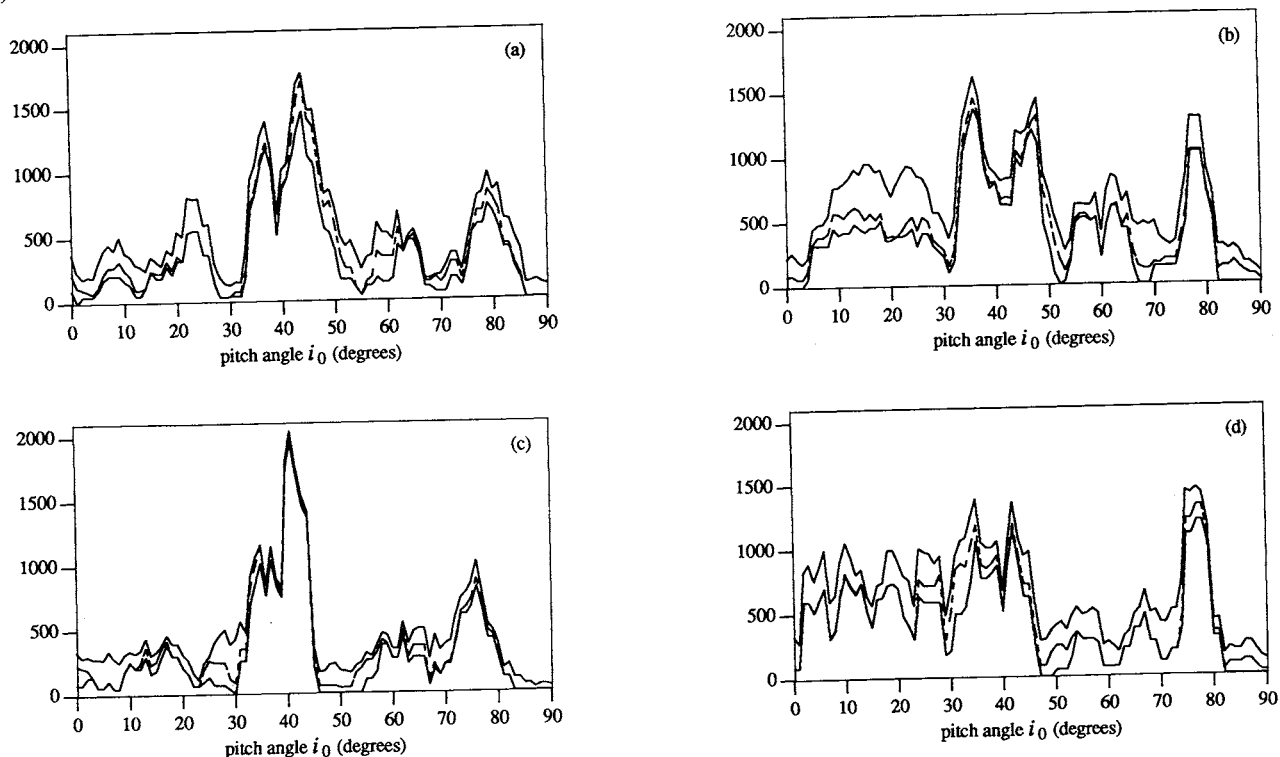


FIG. 4.—Pitch-angle distributions for NGC 1232 weighted by the mass of (number of entities composing) each feature. (a) For the [35- r] case and the a_{toi} partitioning algorithm a majority of the secondary features admit pitch angles between 35° and 45° . This is verified by the [35- r] case with the d_{toi} algorithm (b). Spurs partitioning algorithm a majority of the secondary features admit pitch angles much greater than those of both the global arms and the segments of these arms. Distributions for the [25- r] case combined with the a_{toi} and d_{toi} algorithms shown in (c) and (d) confirm the preference of 35° – 45° values and the peak due to spurs at around 80° . The top curve in each plot depicts the total distribution (i.e., all features modeled between 0° and 90° for all values of ζ in eq. [1] and eq. [2]). The middle curve (*dashed*) considers only spiral loci greater than 1 kpc in length; the lower curve only those loci greater than 1.5 kpc in length. Hence, the bottom curve yields the best information regarding the long, dense features which are consequently the most dominant.

features which are both long and fairly dense exhibit pitch angles in the range 30° and 50° or in a narrower range close to 80° .

Descriptions of two partitioning algorithms were presented in § 2. It would be premature to base conclusions on the results of only one of the two partitioning algorithms. Therefore, the d_{toi} algorithm is also employed to model the features slightly differently in order to ascertain whether, indeed, the distributions obtained so far are biased by numerical modeling.

Figure 3b plots the spiral loci and pitch angles of the more prominent features using the same best fitting log-spiral curve after the d_{toi} algorithm has been employed to partition NGC 1232 into distinct features. Generally, more features tend to be isolated by the d_{toi} algorithm, and those modeled tend to be slightly longer. As a consequence, the height of the associated pitch angle distribution seen in Figure 4b is generally greater than in Figure 4a. More features with pitch angles between 10° and 30° are captured. However the peaks near 35° , 45° , and 80° appear most prominent, consistent with the previous result that many of the features tend to exhibit pitch angles close to these three values.

Turning attention to the [25- r] case shown in Figures 1b, and using the a_{toi} algorithm, the principal spiral loci seen in Figure 3c are obtained. Not as many features are found in the outer regions of the galactic disk (see Fig. 2b). However, some features not modeled in the [35- r] case appear slightly closer to the center (Fig. 3c). Figure 4c shows the distribution of pitch angles. A significant peak dominates near 40° . In addition, secondary peaks near 75° and 35° are evident.

Figure 3d displays prominent spiral loci of features modeled for the [25- r] case after employing the d_{toi} algorithm. Figure 4d suggests the presence of more prominent features with pitch angle in the range below 30° than were exhibited in this case using the a_{toi} algorithm (Fig. 4c). These can be attributed directly to the modeling of more features closer the center, and not so many in outer regions. These features lying closer to the center are usually smaller (due to the space factor of the system), and hence for either partitioning algorithm there is difficulty in defining precisely or realistically the pitch-angle value. Hence, over the nine tolerance values in, say, the d_{toi} algorithm, one sees more variation with these values in turn yielding more noise in the pitch-angle distribution. This is not a quirk in the method since our algorithm captures the physical nature of the feature. Some features however, have a natural tendency toward a more circular shape which can create noise in the pitch-angle distribution.

The fuzzy nature of NGC 1232 combined with the [25- r] algorithm yields a preponderance of features modeled close to the center for which much less confidence can be put in the associated pitch angles. Countering this to a certain extent is the a_{toi} algorithm which emphasizes more of the nucleus of each feature (since the Voronoi areas of the stellar associations which lie on the outer edges are usually quite large and hence eliminated). This can be viewed equivalently as an increase in the ratio of major to minor axes of the elliptical feature. Hence, compared to the d_{toi} algorithm, the a_{toi} algorithm tends to produce more delineated features, but whether more definition implies greater accuracy must still be regarded as an open

question. The a_{tot} algorithm, by capturing only the interior of each of the features, will therefore exclude some in the overall pitch-angle distribution because they are too small. The d_{tot} algorithm however, which definitely retains feature edges, will include all the stellar associations comprising these features and their associated wider variation of pitch angles. Hence we can understand the additional noise in Figure 4d.

In summary, after comparison of Figures 4b and 4d (both of which employed the d_{tot} algorithm), it is evident that sufficient variation in the modeling of prominent features has resulted in discrepancies in pitch angle, which in turn has affected the pitch-angle distributions. Nevertheless, Figure 4d (especially the lower curve which considers features of length > 1.5 kpc) demonstrates that 35° , 45° , and 80° continue to be the preferred pitch-angle values of the principal secondary features.

Having analyzed two versions of NGC 1232 with two different partitioning algorithms, it is apparent that there are three preferred pitch angles for the primary features, that is, 35° , 45° , and $\sim 80^\circ$. Those at 35° and 45° are generally more significant. Although the transformation procedure used may bias the stellar associations included for the analysis, it is evident that including extra stellar associations on the inside of a feature and excluding some outside alters the pitch angle very little. Since the algorithms are designed to give "good approximations" at most, it is concluded that numerical biasing, if any, is insignificant.

It is important to identify and classify the prominent features contributing to each peak in the pitch-angle distribution. Since this is a multiple-armed-type galaxy, it is fairly difficult to distinguish between arm segments and spurs. Weaver (1970) describes spurs as segments which jut out from spiral arms. Elmegreen (1980) adds that they end abruptly and cannot be traced back to the nucleus. A study of those figures which display only the prominent figures along with their pitch angles suggests that most of the secondary features which have been modeled are segments of spiral arms. This can be confirmed by direct comparison with Figure 1. By following along a spiral arm, the prominent segments of the arm branch reveal pitch angles which vary only slightly. This is more apparent in the [35- r] case where more stellar associations in the outer portions of the galactic domain are included in the analysis. The very dense regions of features comprising the spiral arms tend to display pitch angles lying between 30° and 45° . The spiral arms themselves tend to exhibit lower inclinations. This is in agreement with Lynds (1970) who observed that for NGC 1232 the spiraling dark dust lanes appearing on the inside edge of the luminous arm exhibited a pitch angle of approximately 40° .

In spiral galaxy simulations carried out by Roberts et al. (1990, 1992) it was observed that when strong spiral forcing was combined with a significant gas mass fraction, both global spiral structure and local spiral features were present. The global spiral arms were highly disjointed into the local spiral features. These segments of the global arms were oriented outward. In fact, the global arms seemed to consist of a sequence of spiral density inhomogeneities, each with greater orientation than the global arms, and consequently they show good agreement with what has been confirmed mathematically for the observed galaxy NGC 1232 studied here.

The omnipresent peak between 75° and 80° can be attributed mainly to the spur at $\pi/3$ rad (clockwise from north) and 10 kpc from the galactic center (although it might be argued that this is also part of one of the many arm branches). This

spur is both fairly long and dense, and hence modeled for almost all distance tolerances (and area tolerances) in the partitioning algorithms, further indicating its importance. The nucleus of another spur at $2\pi/3$ and 9 kpc also exhibits a pitch angle close to 75° although the complete spur tends to possess a pitch angle of closer to 65° . This is consistent with observations by Elmegreen (1980) that it is common to find two spurs lying at about the same galactocentric radius with similar pitch angles. Furthermore, the spurs identified here appear on the outer edges of the spiral arms and have pitch angles greater than those of the global spiral arms, again consistent with Elmegreen (1980) and Weaver (1970).

Exactly the same analysis is applied to NGC 5457. Figure 5a is the photographic intensity map after application of the non-axisymmetric accentuating factor [35- r]. Immediately we notice that the secondary features are more distinct than those modeled in NGC 1232. The [25- r] case shown in Figure 5b confirms this observation, although, as expected, features toward the outer edge of the galaxy are less well defined. The associated stellar distributions which were analyzed are displayed in Figures 6a and 6b, respectively. The features show greater contrast than those in NGC 1232 and thus are more easily isolated by the partitioning algorithms. Although the same accentuating factors were applied to both external spirals, the reason that the N -body distribution for NGC 5457 is more highly delineated is simple: the original data sample of NGC 5457 showed much greater density contrast between arm and interarm regions than the data sample for NGC 1232. Hence, better delineation of the associated N -body distribution is to be expected for NGC 5457.

The principal spiral loci for the [35- r] case are given in Figure 7a after features were modeled using the a_{tot} method. A comparison of this figure with either Figures 5a or 6a verifies that the primary features have been modeled accurately. Although a completely different partitioning algorithm, the d_{tot} algorithm, was employed to capture the features seen in Figure 7b the prominent spiral loci are almost identical to those in Figure 7a, and their pitch-angle values vary very little. It is most encouraging that both algorithms model the features so similarly. Some additional shorter features nearer to the galactic center have been isolated, however, and can be attributed directly to the nature of the d_{tot} algorithm which tends to model features as slightly longer. Note that only spiral loci greater than the cutoff length (adopted as 1.5 kpc for most features) have been included in these figures. Those present in Figure 7b and not Figure 7a are only just above the cutoff length.

Figures 7c and 7d represent the spiral loci associated with the prominent features modeled for the [25- r] case using the a_{tot} and d_{tot} partitioning algorithms, respectively. Again, the figures bear close resemblance, especially the pitch-angle values of the longer features. The most noticeable difference from the [35- r] case is the omission of the features on the outer edge of the galaxy (where, it should be mentioned, most spurs are located). Overall, however, the long, dense secondary features have all been modeled with similar pitch angles.

The pitch-angle distributions for the [35- r] case in Figures 8a and 8b show the same characteristics. The peak at about 13° is attributed to the two low pitch-angle features identified easily in Figures 7a and 7b. Most of the secondary structure, however, admits pitch-angle values between 30° and 50° . The remaining features in the distributions in Figures 8a and 8b corroborate this observation. Generally, the [25- r] case does

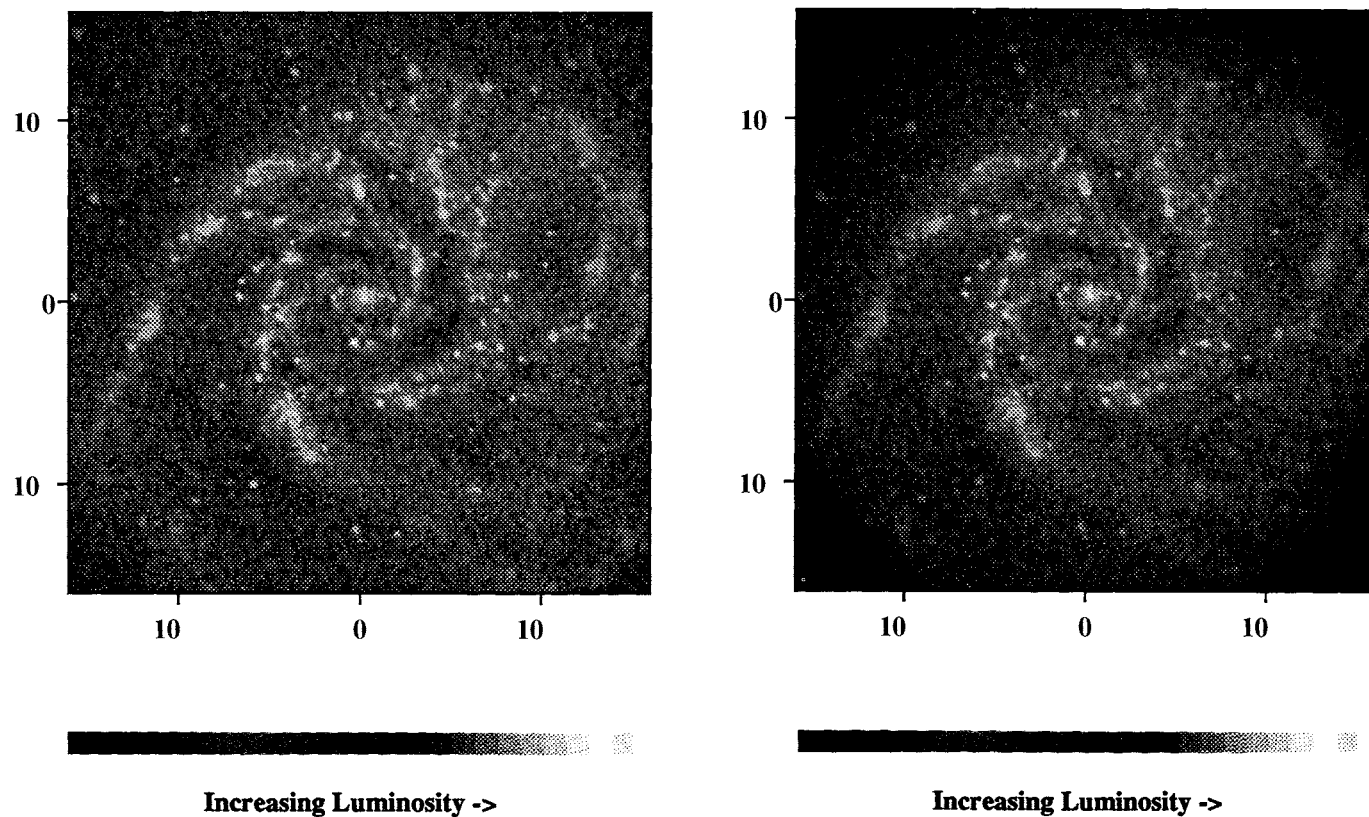


FIG. 5.—Photographic intensity maps of external spiral NGC 5457. The luminosity array (Elmegreen et al. 1990; Elmegreen et al. 1992) is multiplied by (a) $[35-r]$, and (b) $[25-r]$.

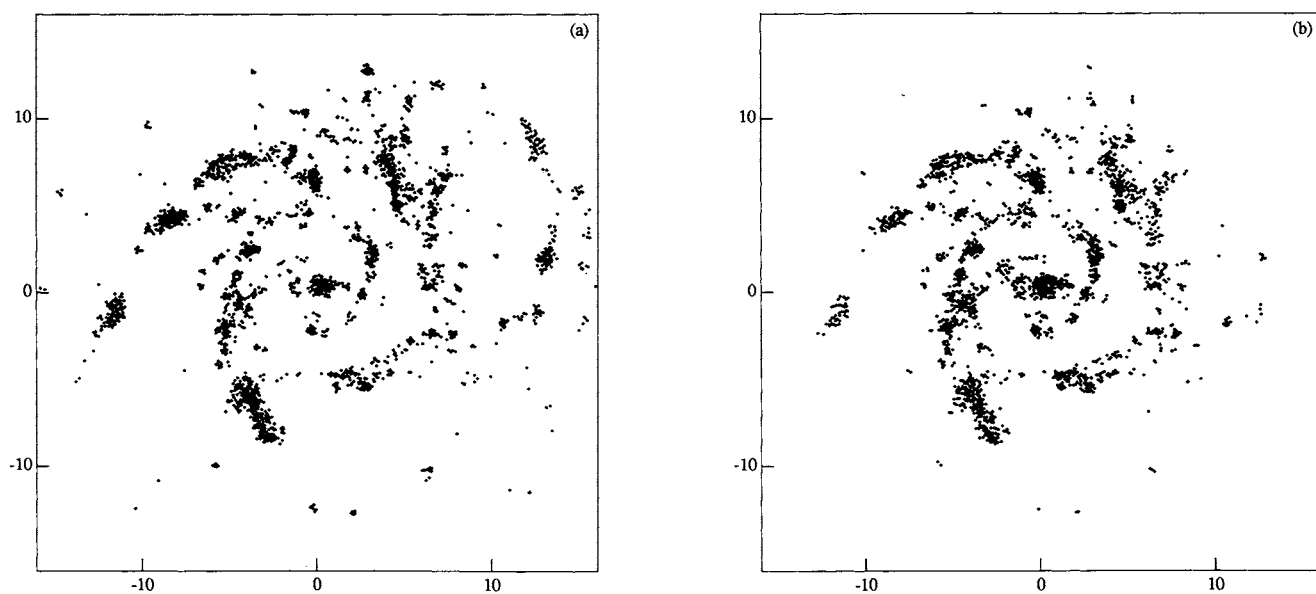


FIG. 6.— N -body distributions of NGC 5457 transformed from Fig. 5 (a) $[35-r]$ case, and (b) $[25-r]$ case. Notice that the density contrast of the secondary features is higher than that seen in NGC 1232. Generally NGC 5457 exhibits greater delineation than NGC 1232.

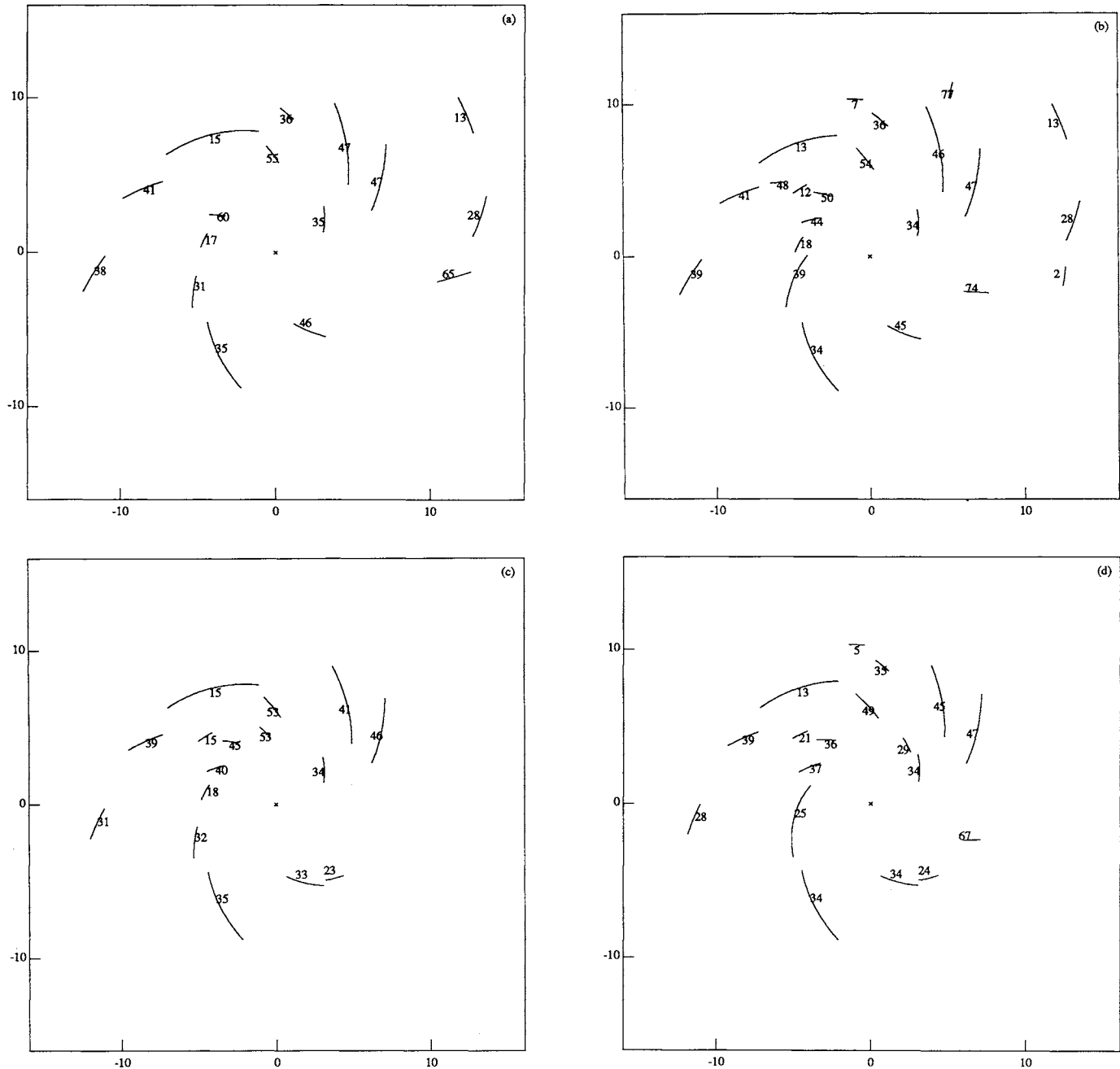


FIG. 7.—Prominent spiral loci modeled in NGC 5457 for the [35- r] case combined with a_{tot} (a), and with d_{tot} (b). (c) and (d) The [25- r] case with a_{tot} and d_{tot} , respectively. Again, all pitch-angle measurements are to the nearest degree.

not model as many features, hence the diminished values at the peaks in Figures 8c and 8d. The split in the primary peak between 40° and 45° in Figures 8a and 8b versus the lack of such a split in Figures 8c and 8d is attributed to three or four features being captured at slightly higher pitch-angle values for both the a_{tot} and d_{tot} algorithms. The noise is damped in NGC 5457 because although the [35- r] case picks up less information toward the center, the features modeled remain highly delineated. Therefore, their modeled pitch-angle values are easily calculated, and we can be confident that these results are of a physical nature. Of course, for the [25- r] case these fea-

tures are equally well defined for both the a_{tot} and d_{tot} partitioning algorithms.

4. CONCLUSIONS AND DISCUSSION

A numerical method, originally developed to analyze the morphology of global and local structure in prototype galaxies (Russell & Roberts 1992), is modified for analyzing observed disk-shaped galaxies. Two digitized spiral galaxies NGC 1232 and NGC 5457, with varying degrees of contrast between arm and interarm regions, serve as the representative candidates for this analysis.

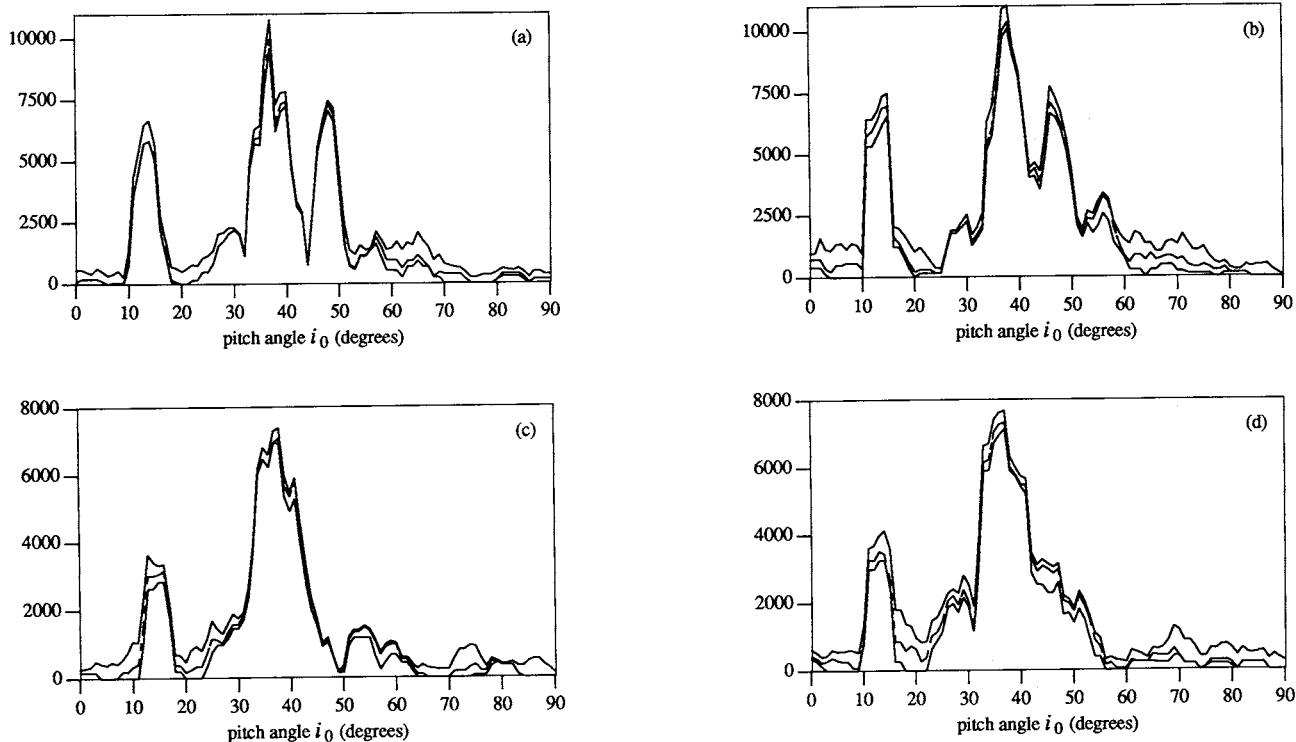


FIG. 8.—NGC 5457 pitch-angle distributions associated with the [35- r] case and a_{tot} partitioning algorithm (a) and d_{tot} algorithm (b). (c) and (d) The [25- r] case combined with the a_{tot} and d_{tot} algorithms. Notice the preference of the secondary structure to the 35°–50° pitch angle values, very similar to the pitch angle distributions for NGC 1232.

One sees from these results that a multiple-armed spiral galaxy does not necessarily have to exhibit a distribution of features over the whole spectrum of pitch angles. Indeed, the evidence from the distributions presented in Figures 4a, 4b, and 4c for NGC 1232 suggests that the majority of the prominent features admit pitch angles in the range between 30° and 50°, with some high pitch-angle spurs in the range near 80°. For NGC 5457 it is even more clear that the majority of the prominent features admit pitch angles in the range between 30° and 50°. The model simulations of flocculent-type galaxies of Roberts et al. (1992) also predict similar types of pitch-angle distributions (Russell & Roberts 1992).

For NGC 5457, it is apparent that pitch-angle values of the principal features lie in the same regimes for both [35- r] and [25- r] cases and for both a_{tot} and d_{tot} algorithms. The preference to the 30° to 50° range is of considerable interest. These pitch-angle distributions are more clearly defined than those seen for NGC 1232 simply because the N -body distribution for NGC 5457 is more clear cut. On examination of the global structure of NGC 5457 one sees that the global arms, although moderately disjointed, clearly have pitch angles near 30°. Hence, many of the features captured are spurs and feathers of the types which have been identified by Elmegreen (1980) to have pitch angles greater than those of the global arms. Arm segments near a global arm may be undergoing rotation outward due to reverse shear (Balbus 1988). Other arm segments separated sufficient distances from a major global arm may be undergoing restoration from such outward-rotated orientations as well as elongation due to overall galactic shear.

Elmegreen (1980) selected five features in the outer parts of NGC 5457, identified them as spurs, and estimated the pitch angles as 74° (spur 1), 60° (spur 2), 64° (spur 3), 68° (spur 4), and

72° (spur 5). It is interesting that our automated algorithms herein capture as many as four of these five features as high-pitch-angle spurs. As illustrated, for example, in Figure 7b, the pitch angles of these four features are determined as: 48°–50° (spur 1), 54° (spur 2), 47° (spur 3), and 77° (spur 4). Thus, the automated algorithms developed herein yield pitch angles that are somewhat lower than those estimated by Elmegreen (1980) for three of the four features: 48°–50° vs. 74° (spur 1), 54° vs. 60° (spur 2), and 47° vs. 64° (spur 3). Note that the difference for spur 3 can be attributed to the fact that the automated algorithms closely fit matter in the spur as well as a portion of the global arm from which it protrudes, whereas Elmegreen considers only the highly angled extension. For the fourth feature, the automated algorithms yield a pitch angle that is somewhat higher than that estimated by Elmegreen (1980): 77° vs. 68° (spur 4).

The reason underlying the lack of inclusion of the fifth feature could be in part due to the fact that the N -body distributions employed in our analysis tend to omit stellar associations on the outer edge of the galaxy where most spurs can be most easily identified. Furthermore, spurs tend to be narrow and therefore fairly sparse, and hence are treated in our analysis as insignificant compared to the longer, denser, more prominent features. Indeed, the fifth feature is the outermost one of the five features selected by Elmegreen (1980). It appears less conspicuously than the other four features in the image data in Figures 5a and 5b. Furthermore, its constituent stellar associations in Figures 6a and 6b appear clumped into two separate groups and consequently not sufficiently contiguous for the feature as a whole to be defined by the algorithms as a spur.

In addition to the five spurs identified by Elmegreen (1980),

our automated algorithms identify other features of high pitch angle in NGC 5457: 60° and 65° (Fig. 7a), 74° (Fig. 7b), 53° (Fig. 7c), and 67° (Fig. 7d). Comparisons of all the high-pitch-angle loci in Figure 7a with the image data in Figure 5 and the resultant stellar associations in Figure 6 illustrate the closeness of the automated fits obtained.

One of the main objectives of this work is to determine if the model could decipher the differences in pitch-angle distributions for fuzzy versus well-defined secondary galactic structures. It now appears that this goal is attainable. An obvious question follows: Is it possible to apply this method to a whole cross section of flocculent-type multiple-arm spiral galaxies and use the resulting pitch-angle distributions to determine a classification scheme for such systems? Indeed, this is posed as the next step in future work. If it were possible to gather data samples similar to those analyzed here for a selection of spiral galaxies, the automated mathematical method could prove to be a powerful tool, possibly even a classification device, to uncover pitch-angle properties of the spectrum of secondary features occurring in both real and prototype spiral galaxies. We realize nevertheless that there may be some biasing due to the method of producing the N -body distributions. However,

we already have confidence in the results for NGC 5457, even though the fuzziness of NGC 1232 does raise some cause for concern. One must remember that the primary objective is to determine whether this method, originally developed for analyzing prototype galaxy cases, could be used on these observed external spirals. We do realize that in order to use this as a classification scheme and to eliminate any biasing, the development of a parallel algorithm might well be required which could deal directly with an array of luminosities rather than an N -body distribution.

We thank Bruce Elmegreen for kindly providing us with the data samples for NGC 1232 and NGC 5457 prior to publication. This work was supported in part by the National Science Foundation under grant AST-87-12084 and grant DMS 91-06029, and NASA under grant NAGW-929. The computations were carried out on the AMSUN cluster, the IBM RS 6000s, and the CDC 855 at the University of Virginia, the CRAY Y-MP at the Pittsburgh Supercomputing Center under grant AST 880019P, and the SGI Indigos at NASA Goddard Institute for Space Studies in New York.

REFERENCES

- Adler, D. S., & Roberts, W. W. 1992, *ApJ*, 384, 95
 Balbus, S. A. 1988, *ApJ*, 324, 60
 Brostow, W., Dussault, J.-P., & Fox, B. L. 1978, *J. Comput. Phys.*, 29, 81
 Dirichlet, G. L. 1850, *Z. Reine Angew. Math.*, 40, 216
 Elmegreen, B. G., Elmegreen, D. M., & Montenegro, L. 1992, *ApJS*, 79, 37
 Elmegreen, B. G., Elmegreen, D. M., & Seiden, P. E., 1990, private communication
 Elmegreen, D. M. 1979, *ApJS*, 43, 37
 ———. 1980, *ApJ*, 242, 528
 Lynds, B. T. 1970, in *IAU Symp. 38, The Spiral Structure of Our Galaxy*, ed. W. Becker & G. Contopoulos (Dordrecht: Reidel), 26
 Roberts, W. W., & Adler, D. S. 1989, in *App. of Comp. Tech. to Dyn. Astr.*, ed. P. K. Seidelmann & J. Kovalevsky (Dordrecht: Kluwer), 285
 Roberts, W. W., Adler, D. S., Lowe, S. A., & Lin, C. C. 1992, *ApJ*, submitted
 Roberts, W. W., Lowe, S. A., & Adler, D. S. 1990, in *Ann. NY Acad. Sci.* 596, Galactic Models, ed. J. R. Buchler, S. T. Gottesman, & J. H. Hunter, Jr., 130
 Russell, W. S. 1991, Ph.D. thesis, Univ. Virginia
 Russell, W. S., & Roberts, W. W. 1992, *ApJ*, submitted
 Voronoi, G. 1908, *Z. Reine Angew. Math.*, 134, 198
 Weaver, H. F. 1970, in *IAU Symp. 39, Interstellar Gas Dynamics*, ed. H. Habing (Dordrecht: Reidel), 22